Automatic Detection and Characterization of Biomarkers in OCT Images

Melinda Katona[1], Attila Kovács[4], László Varga[1], Tamás Grósz[2], József Dombi[3], Rózsa Dégi[4], László G. Nyúl[1]

[1]Department of Image Processing and Computer Graphics, University of Szeged
[2]MTA-SZTE Research Group on Artificial Intelligence, University of Szeged
[3]Department of Computer Algorithms and Artificial Intelligence, University of Szeged
Árpád tér 2, H-6720, Szeged, Hungary
{mkatona, vargalg, groszt, dombi, nyul}@inf.u-szeged.hu
[4]Department of Ophthalmology, University of Szeged
Korányi fasor 10-11, H-6720, Szeged, Hungary
{kovacs.attila, degi.rozsa}@med.u-szeged.hu

Abstract. Optical Coherence Tomography (OCT) is one of the most advanced, non-invasive method of eye examination. Age-related macular degeneration (AMD) is one of the most frequent reasons of acquired blindness. Our aim is to develop automatic methods that can accurately identify and characterize biomarkers in OCT images, related to AMD. We present methods for quantizing hyperreflective foci (HRF) with deep learning. We also describe an algorithm for determining pigmentepithelial detachment (PED) and localizing outer retinal tubulation (ORT) that appears between the layers of the retina.

Keywords: age-related macular degeneration, biomarker, pigmentepithelial detachment, hyperreflective foci, outer retinal tubulation, optical coherence tomography

1 Introduction

Age-related Macular Degeneration (AMD) is a health problem worldwide, that is the leading cause of vision loss in the Western World. While symptoms are rare in patients below 50 years of age, an increasing prevalence of AMD can be detected in the elderly population. AMD means degeneration of the macula, the region of the retina responsible for central vision. Since only this specific part of the retina is affected by AMD, untreated patients lose their fine shape- and face recognition, reading ability, and central vision [4]. AMD can be divided into two subtypes; the dry (non-exudative) and the wet (exudative, neovascular) form. The latter one causes rapid and serious visual impairment and accounts for 10% of the cases. In this more acute, neovascular type of the disease, abnormal angiogenesis causes fluid and blood leakage into the retinal layers thus resulting in photoreceptor lesion. Albeit the exact pathomechanism of the disease is still

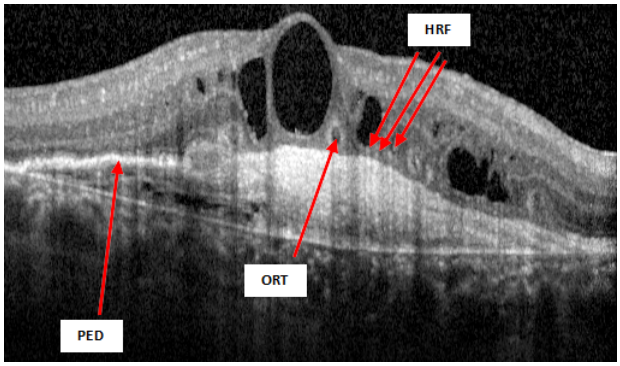

Fig. 1. Optical Coherence Tomography (SD-OCT) image of the retina with biomarkers

unclear, it is known that the vascular endothelial growth factor (VEGF) plays crucial role in the pathogenesis [10]. The first choice of treatment in neovascular AMD is anti-VEGF intravitreal injection, a periodic injection into the eye.

During the last decade, optical coherence tomography (OCT) has become a basic tool in diagnosing and monitoring neovascular AMD and its response to anti-VEGF treatment. With the help of OCT, we are capable of detecting the layers of the retina, and also the effects of the disease, the so-called OCT biomarkers, such as subretinal/intraretinal fluid accumulation, pigmentepithelial detachment (PED), outer retinal tubulation (ORT) or hyperreflective foci (HRF) (Fig. 1). These markers help the clinical decision-making process for observing/treating/re-treating a patient. To improve the treatment procedure, there is a need for more precise measurements, hence our aim was to create algorithms which can automatically identify and quantify some of the above mentioned biomarkers, namely PED, ORT and HRF.

A large number of publications in the scientific literature deal with cysts, subretinal fluid detection and retinal layer segmentation, however only a small number of papers are available on PED. Haq et al. [3] defined 12 retinal layer with a multi resolution graph-search method and the PED was calculated from the relative position of the lower two layers. The algorithm of Shi et al. [9] applied machine learning for PED detection. We have not come across any papers about automatic segmentation of ORT. In case of the HRFs there are some simple techniques for the detection (see, e.g., [8]), but we have not found any methods in use related to AMD.

2 Materials and methods

In this section, we present several algorithms to detect HRF, PED and ORT. The OCT images were acquired using Heidelberg Spectralis (Spectralis, Heidelberg Engineering, Heidelberg, Germany) OCT scans on wet age-related macular degeneration. Patients were either treated naively or with anti-VEGF intravitreal

injections. The annotated images contained many biomarkers, such as subretinal fluid, PED, subretinal and hyperreflective material. The currently used data consist of images of different patients taken at different times. All image sequences consisted of 49 slices taken with a 6×6 mm pattern size and $122\,\mu$m slice distance. The slices were generated by averaging 30 frames on each B-scan. Slices had a resolution of 512×496 pixels with pixel sizes 11.45 and $3.87\,\mu$m and a quality score above 16 dB.

We evaluated our PED and ORT segmentation method by comparing the results to manual segmentations of ophthalmologists for 2 image sequences. The database of HRF consisted of 11 image sequences taken from 7 clinical patients. The annotation was performed by two clinical doctors, independently marking the hyperreflective foci.

2.1 PED detection and ORT localization

Pigment epithelium detachment (PED) can be an important medical feature of the disease. PED estimation can be made relatively easily after the retinal pigment epithelium (RPE) layer is detected. Determining the outer boundaries, such as the internal limiting membrane (ILM) and RPE layers are defined in our previous work [5]. We calculated a possible normal layer boundary using the known RPE boundaries to characterize the detachment. We took 1% of the points from both sides of the image and we fitted a smoothed cubic spline to these points, giving the possible boundary.

In many cases, even for doctors, it is difficult to see the ORTs, they can only guess their place and extent. Consequently, an approximate segmentation result can also help.

The ORT has hyperreflective contour and contains hyper- hyporeflective points. The procedure is based on finding hyperreflective points. As we can see in Fig. 1, the input image is noisy, so we used a Wiener filter with a 3×5 pixel kernel. Our input image size was 509x496, so a smaller kernel was sufficient. Reflective points were localized using a Hessian detector [1]. Then, we performed a non-maximum suppression and considered the 100 highest points. The result image may also contain a several points that are not relevant for ORT localization.

For filtering the false points, we used some prior information about the biomarkers. Firstly, we calculated the retina thickness and we kept only those points which are located in the lower third of the retina. Since we know that ORT is close to the RPE layer and in the distorted retina region or nearby surroundings, by estimating the beginning and end of the distortion on the slices additional points can be removed. We used our published algorithm [5] to detect the extent and location of the distortion of the retina and the detection of cyst and liquid areas. Limiting the specific extent of the ORT in many cases is very difficult, because there is no clear distinction between the hyperreflective wall and its surroundings. We performed adaptive histogram equalization in the image so that at least a part of the possible contours became separable by hysteresis thresholding. The two threshold values are given as the lower and upper third

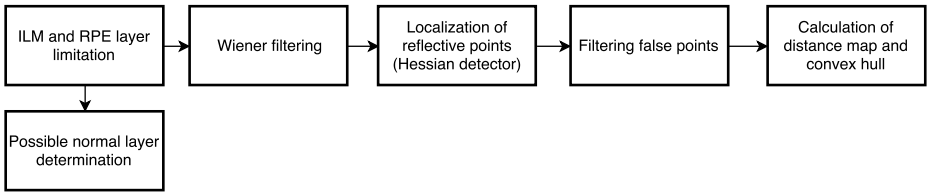

Fig. 2. Flowchart of the proposed PED detection and ORT localization algorithm.

of the maximum intensity value in the image. At the end of the last filtering, we kept only those points which were part of an object in the binary image. Then, we calculated distance map for the points, thresholded and finally computed the convex hull of the objects. he key stages of the procedure are summarized in Figure 2.1.

2.2 Quantifying change in HRFs using Deep Neural Networks

One of the aims of this work was to quantify the number of HRF pixels in the OCT slices. Although this included the segmentation of HRF pixels, our goal was not a detection, but rather the tracking slight changes in the amount of HRFs. This can help the doctors to objectively track the progress of the disease and aid the treatment planning. For this task, we used Deep Neural Networks (DNNs), which were trained using annotated images by ophthalmologists.

We applied several types of networks, namely the standard Artificial Neural Networks with one hidden layer, Deep Rectifier Neural Networks (DRNs) [2] and Convolution Neural Networks (CNNs) [7], which were successfully used in many previous medical studies [6]. The goal of these networks was to classify one single pixel from a given feature vector. The full image classification was performed by classifying each pixel of the image, seperately. We gave the networks two types of input data. The first one was the raw pixel data, which consisted of raw pixel intensities in 25 $\times$ 25 pixel vicinity of the pixel to classify. The other type of input consisted of feature vectors extracted from the OCT images. These features were:

- Weighted sum of pixel intensities in the neighborhood weighted with a Laplacian of Gaussian (LoG) kernels of different σ values. LoG filter σ value ranged from 1 to 2 with a step of 0.1;
- Distance of the pixel from the ILM and RPE layers;
- Distance from subretinal fluid;
- To help the networks recognize shadows of veins we added 25 average intensity values of 40 pixel long vertical strips under the pixel in question, i.e., $\left\{\sum_{j=1}^{40} I(x-i, y-j) \;\;,\;\; i \in \{-12, -11, \ldots, 11, 12\}\right\}$, where $I(x, y)$ is the pixel of question with x and y coordinates.

The marked targets by ophthalmologist were the bright spots of the images having equal or higher reflectivity than the RPE band, and a diameter of approximately $20 - 40\mu m$ (2-4 pixels). The annotation consisted of the delineation the HRF pixels of the slices. Before the training phase, we separated the dataset into two partitions, 7 out of 11 sequences were used for training the networks. The other 4 sequences were kept for testing. The images in the test set were taken from 4 different patients. The data of these patients were not included in the training dataset in any way (i.e., the training data set was taken from other patients). Within the training dataset, we used 1 out of every 7 slices for development purposes (i.e. hyperparameter tuning).

We trained an ANN and a DRN using only the pixel data. Furthermore, we also changed the network structure by splitting the first hidden layer of the DRN; half the neurons were connected to the raw pixel input and the other half was connected only to the extracted features.

The structure of the networks were determined empirically by seeking the structures giving the best results. The ANNs had only one hidden layer and 7000 hidden neurons, the DRNs had 5 hidden layers each having 1000 rectifier neurons. To train the ANNs and the DRNs we applied stochastic gradient descent (i.e. backpropagation) training with a mini-batch size of 100. The initial learn rate was set to 0.001, which was halved after each iteration if the performance on the validation set did not improve. During the preliminary experiments we found that the optimal value of the sampling parameter (λ) was 0.8.

The CNN had 3 convolutional layers having a kernel size of 5×5 and output size of 32, 32 and 64, respectively, followed by a fully connected layer of 2 neurons, and a softmax layer. The CNN was trained with backpropagation method with a fixed learning rate of 0.001, momentum of 0.9, and weight decay of 0.004. The batch size was 128. Before training and evaluation we normalized the data to the interval $[-1, 1]$. The net was initialized with random values of uniform distribution, and we did not use any pre-training.

3 Evaluation and results

3.1 PED and ORT detection

For calculating accuracy, we used the Jaccard coefficient of similarity, which measures the overlap of the annotated segment and the detected biomarker region. The result of the pigmentepithel detachment localization depends on the location of the pre-determined RPE layer. It may also appear as subretinal hyperreflective material, which is not distinguished from the detachment, so this appears as a false detected region in evaluation. Figure 3 represent the Jaccard values for the two annotated sequences. It can be concluded that the procedure in most cases closely approximates the PED area designated by the ophthalmologist.

In the case of ORT, we analyse the result in two different ways, because not only the localization is important for the ophthalmologist, but sometimes it is also appropriate to determine, if ORT appears on images or not. We achieved a

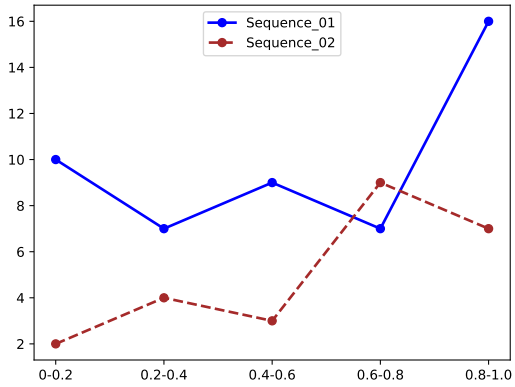

Fig. 3. Jaccard histogram of 2 image sequences. Horizontal axis represents Jaccard values and vertical axis is the number of slices with Jaccard index falling into the given ranges.

Jaccard value of 0.530 for the two sequences, but we filtered images which do not contain ORT with 97.6% success. Figure 4 illustrates the results of the proposed methods.

Running time of the method was 0.401 ms, PED detection was 0.006 ms on average and ORT localization took 0.091 ms per slice.

3.2 Tracking the amount of HRFs

The small size and the limited amount of the HRFs made the use of simple (F1 score, or Dice coefficient-based) pixel-wise evaluation metrics meaningless, since only a 1 pixel misalignment in the segmentation would show significant error on the 2-4 pixel sized HRFs while the result is still useful. Also, segmenting HRF-s was not the goal of this study as the doctors wanted a method to track the changes in the HRF amounts. For the comparison, we evaluated the performance of the nets by calculating the Pearson's correlation coefficient between the number of HRF pixels on the automatic and manual segmentations. Using 196 slices, we pairwise compared the pixel counts got by the automatic segmentations to those of the gold standard annotation. As a baseline for the study, we also calculated the correlation between the manual annotations of the two doctors. The results can be seen in Table 1.

We argue, that if a neural network can reach a higher correlation than the one between the annotations of the doctors (0.812), then its outputs are useful, since they reflect the number of HRFs on a slice as well as the annotation of a medical expert would. In most of the cases, the networks were able to provide good results as almost all of them achieved a correlation value above

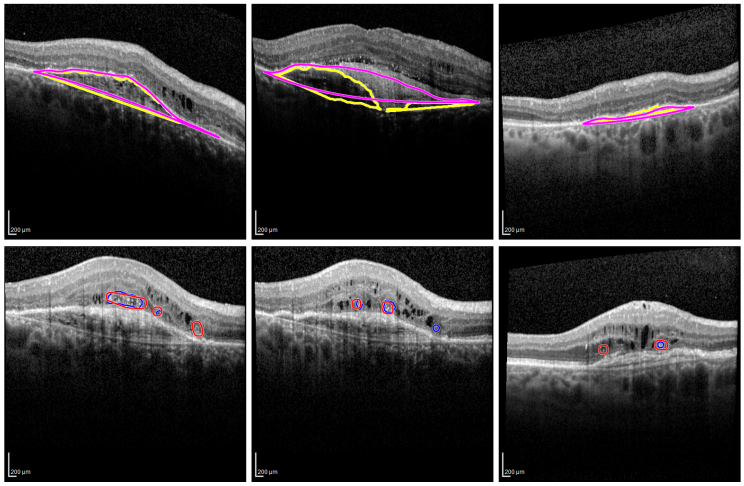

Fig. 4. Illustration of detected and annotated PED and ORT. Upper images show PED regions (magenta - detected, yellow - annotated) and lower pictures represent ORT (red - detected, blue - annotated).

Table 1. Pearsons correlation coefficient between the automatic and manual segmentations. In columns one can see the comparison of segmentations sources (NN - Neural network; MD.# - physician).

Data (optimizer goal)	NN ⇔ MD.1	NN ⇔ MD.2	MD.1 ⇔ MD.2
ANN - pixel (accuracy)	0.778	0.789	0.812
ANN - pixel&feature (accuracy)	0.698	0.775	
DRN - pixel (accuracy)	0.812	0.783	
DRN - pixel&feature (accuracy)	0.796	0.782	
split DRN - pixel&feature (accuracy)	0.812	0.790	
DRN - pixel&feature (dice)	0.802	0.788	
CNN - pixel (accuracy)	0.845	0.862	

0.78. Interestingly, using the extracted features did not improve the quality of the segmentation, suggesting that the nets learned to extract those informations from the raw data. Furthermore, switching the loss function to the Dice loss was neither beneficial.

The best results were achieved by the CNN, with correlation coefficients over 0.845. This indicates that it can produce an acceptable, and reliable quantization. We should also note that the hand made full delineation of HRFs in an OCT sequence leading to an accurate quantization is time consuming, and our method can give a quick automatic estimation of the amount of HRFs.

Based on the above results, we can say that our methods are capable of tracking the number of HRFs in OCT images, and they could aid the doctors during the planning of the treatment, by speeding up the decision making process.

4 Conclusions

We have described procedures for analysing some OCT features of AMD patients. The methods include detection of PED, localization of ORT between retinal layers, and the quantization of HRF. We determined the possible normal layer boundary for the characterization of PED and we introduced a method to localize ORT. We compared our results with the annotated data by medical colleagues. Furthermore, automatic detection of these specified biomarkers can be used not only in AMD patients, so it can help the doctor during patient examination.

Our HRF quantization method achieved a correlation coefficient as good as the one between the annotations by the ophthalmologists. Hence, we argue that they are suitable for aiding the diagnosis and treatment planning process.

5 Acknowledgements

We would like to thank the NVIDIA Corporation for the donation of the Tesla K40 GPU used for this research. Tamás Grósz was supported by the ÚNKP-17-3 New National Excellence Programme of the Ministry of Human Capacities.

References

1. Beaudet, P.: Rotationally invariant image operators. In: International Joint Conference on Pattern Recognition, Kyoto, Japan. pp. 579–583 (1978)
2. Glorot, X., Bordes, A., Bengio, Y.: Deep sparse rectifier neural networks. In: Proceedings of the Fourteenth International Conference on Artificial Intelligence and Statistics. vol. 15, pp. 315–323. PMLR (2011)
3. Haq, A., Wilk, S.: Detection of wet age-related macular degeneration in oct images: A case study. In: Innovations in Biomedical Engineering. pp. 43–51. Springer International Publishing (2018)
4. Hee, M.R., et al.: Optical Coherence Tomography of Age-related Macular Degeneration and Choroidal Neovascularization. Ophthalmology 103(8), 1260–1270 (1996)
5. Katona, M., Kovács, A., Dégi, R., Nyúl, L.G.: Automatic detection of subretinal fluid and cyst in retinal images. In: Image Analysis and Processing - ICIAP 2017, Proceedings, Part I. pp. 606–616 (2017)
6. Kayalibay, B., Jensen, G., van der Smagt, P.: CNN-based Segmentation of Medical Imaging Data. CoRR abs/1701.03056 (2017)
7. Krizhevsky, A., Sutskever, I., Hinton, G.E.: Imagenet classification with deep convolutional neural networks. In: Advances in Neural Information Processing Systems 25, pp. 1097–1105 (2012)
8. Mokhtari, M., Kamasi, Z.G., Rabbani, H.: Automatic detection of hyperreflective foci in optical coherence tomography b-scans using morphological component analysis. In: 2017 39th Annual International Conference of the IEEE Engineering in Medicine and Biology Society (EMBC). pp. 1497–1500 (July 2017)
9. Shi, F., et al.: Automated 3-d retinal layer segmentation of macular optical coherence tomography images with serous pigment epithelial detachments. IEEE Transactions on Medical Imaging 34(2), 441–452 (2015)
10. Velez-Montoya, R., et al.: Current knowledge and trends in age-related macular degeneration: today's and future treatments. Retina 334, 1487–1502 (2013)